2013 IEEE/RSJ International Conference on
Intelligent Robots and Systems (IROS)
November 3-7, 2013. Tokyo, Japan

A Robust Sonar Servo Control Scheme for Wall-Following using an Autonomous Underwater Vehicle

George C. Karras[1], Charalampos P. Bechlioulis[1], Hashim Kemal Abdella[2], Tom Larkworthy[2], Kostas Kyriakopoulos[1] and David Lane[2]

Abstract— **This paper describes the design and implementation of a model-based sonar servoing control scheme for Autonomous Underwater Vehicles (AUVs). The proposed controller is designed for autonomous surveillance of underwater structures and it is robust against external disturbances and parametric uncertainties in the AUV dynamic model. The sensor suite includes a Multi-beam Imaging Sonar which provides measurements to a RANSAC-based algorithm for structure detection and pose estimation of the vehicle with respect to the structure. The sonar-based pose estimation is properly fused with the rest of the state measurements provided by a navigation module and the resulted state vector is incorporated as feedback to the controller. The proposed control scheme has analytically guaranteed stability and convergence properties, while its applicability and performance are experimentally verified using the Nessie VI AUV in the presence of external disturbances (medium height waves).**

I. Introduction

Autonomous underwater vehicles usually operate under difficult circumstances and perform complex tasks such as ship hull inspection, surveillance of underwater facilities (e.g., oil platforms, propulsion systems, etc) and handling of underwater equipment (e.g control panels, valves). These tasks mainly require robust motion control systems as well as a detailed description of the environment. Motion control for underwater vehicles has been an active research field for the past two decades. It is based on a variety of design techniques such as PID control, linear quadratic optimal control, nonlinear control, H_∞ control and neural/fuzzy control (see [1]–[3] and the references therein). In the majority of the aforementioned techniques dynamic models are used to design model-based control systems in an attempt to incorporate the dynamic properties and limitations of the vehicle in the control design to obtain robust performance.

Moreover, the measurements delivered by the sensor suite, must be used simultaneously both for accurate map building of the workspace as well as state feedback for the motion control scheme. A sensor able to meet such requirements in an acoustic environment is imaging sonar. The development of sophisticated acoustic image processing techniques, allow us to integrate these type of sensors to the navigation module

This work was supported by the EU funded project PANDORA: Persistent Autonomy through learNing, aDaptation, Observation and RePlAnning", FP7-288273, 2012-2014.

[1]School of Mechanical Engineering, National Technical University of Athens, Athens 15780, Greece {karrasg, chmpechl, kkyria}@mail.ntua.gr.

[2]Ocean Systems Laboratory, Heriot-Watt University, EH14 4AS Edinburgh, UK {hashmekelle, tom.larkworthy}@gmail.com, D.M.Lane@hw.ac.uk.

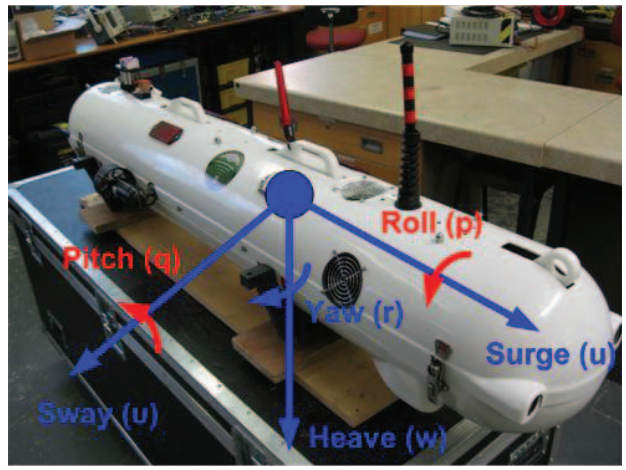

Fig. 1. Nessie VI AUV. Blue color indicates actuated DOFs. Red color indicates unactuated DOFs.

of AUVs, contributing in that way not only to the detailed description of the environment but also to the autonomous navigation of the vehicle. The incorporation of acoustic imaging data to the motion control of a robotic system [4]–[9], is called sonar servoing, similarly to visual servoing when data from visual sensors (e.g cameras) are used to minimize the control error function.

Sonar servoing is successfully incorporated in the wall inspection task of Kazmi *et al.* [10]. The raw sonar data is preprocessed using a low-pass filter to remove the backscatter noise. Among the various smoothing filters available, Tena Ruiz *et al.* [11] argue that the median filter performs better in removing the noise arising from the backscattering effect. However, Trucco *et al.* showed in [12] that the median filter can be approximated using a 7×7 Gaussian filter at a minimal computational cost. In most real time applications the smoothed image is segmented using a threshold technique. Then, it is fed to a line fitting algorithm for determining the exact location of the line/wall. A review of various line fitting algorithms for 2D range data is presented in [13], where the authors showed that the least square techniques are highly influenced by outliers, while a standard hough transform doesn't take noise into account. At last, Random Sample and Consensus (RANSAC) is suggested as a better algorithm in considering noise while also minimizing the effect of outliers.

This paper describes the design and implementation of a sonar servo control scheme for surveillance tasks using

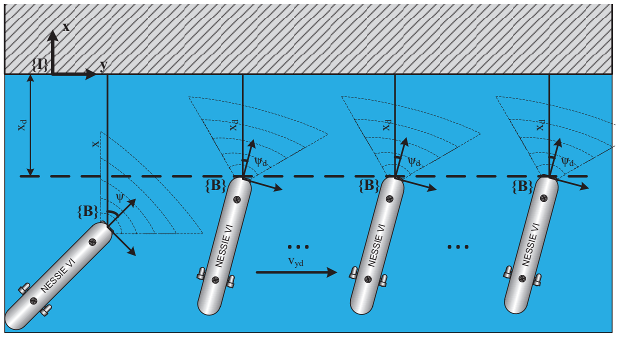

Fig. 2. The wall following problem.

an AUV. A Multibeam Imaging Sonar is integrated with the vehicle's sensor suite. The acoustic measurements are appropriately filtered using a RANSAC algorithm and the relative position and orientation of the vehicle with respect to the surface under surveillance are calculated. A sensor fusion algorithm is responsible for integrating the sonar measurements with the state vector provided by the rest of the sensor suite which consists of a Doppler Velocity Log Sensor (DVL), a Fiber Optic Gyro (FOG) and a depth sensor. The estimated state vector is then incorporated as feedback to the model-based motion control scheme. The proposed controller is robust against external disturbances as well as to parametric uncertainties in the AUV dynamic model. The resulting control scheme has analytically guaranteed stability and convergence properties, while its applicability and performance are experimentally verified using the Nessie VI AUV in the presence of external disturbances (medium height waves).

The rest of the paper is organized as follows: Section II describes the proposed methodology, including the wall detection by the sonar, the sensor fusion algorithm and an analytical description of the motion control design. Section III illustrates the efficiency of our approach through an extensive experimental procedure. Section **??** gives a small description of the accompanying experimental video. Finally, Section IV concludes the paper.

II. Methodology

A. Problem Formulation

The vehicle used in this work is the Nessie VI AUV (Fig. 1), which is modeled as a rigid body subject to external forces and torques. Let $\{I\}$ be an inertial coordinate frame on the wall to be inspected with the x and z axis showing inwards and downwards respectively, and $\{B\}$ a body-fixed coordinate frame whose origin O_B is located in front of the vehicle at the sonar sensor (see Fig. 2). Furthermore, let $\eta_1 = [x, y, z]^T$ be the position and $\eta_2 = [\phi, \theta, \psi]^T$ be the orientation of O_B in $\{I\}$ with ϕ, θ, ψ denoting the roll, pitch and yaw angles. Let $\mathbf{v}_1 = [u, v, w]^T$ be the linear velocity (i.e., the longitudinal (surge), transverse (sway) and vertical (heave)) of O_B with respect to $\{I\}$ expressed in $\{B\}$ and $\mathbf{v}_2 = [p, q, r]^T$ be the angular velocity (roll, pitch, yaw) around the longitudinal, transverse and vertical axis respectively. Hence, the kinematic equations of motion can be written as:

$$\dot{\eta} = \begin{bmatrix} \dot{\eta}_1 \\ \dot{\eta}_2 \end{bmatrix} = \mathbf{J}(\eta)\,\mathbf{v} = \begin{bmatrix} \mathbf{J}_1(\eta_2) & \mathbf{0}_{3\times3} \\ \mathbf{0}_{3\times3} & \mathbf{J}_2(\eta_2) \end{bmatrix} \begin{bmatrix} \mathbf{v}_1 \\ \mathbf{v}_2 \end{bmatrix} \quad (1)$$

where $\eta = \left[\eta_1^T, \eta_2^T\right]^T$ and $\mathbf{v} = \left[\mathbf{v}_1^T, \mathbf{v}_2^T\right]^T$ are the generalized position/orientation and velocity vectors and $\mathbf{J}(\eta)$ is the generalized Jacobian matrix transforming the velocities from the body-fixed to the earth-fixed frame defined as:

$$\mathbf{J}_1(\eta_2) = \begin{bmatrix} c\psi c\theta & c\psi s\theta s\phi - s\psi c\phi & c\psi c\phi s\theta + s\psi s\phi \\ s\psi c\theta & s\phi s\theta s\psi + c\psi c\phi & s\theta s\psi c\phi - c\psi s\phi \\ -s\theta & c\theta s\phi & c\theta c\phi \end{bmatrix}, \quad (2)$$

$$\mathbf{J}_2(\eta_2) = \begin{bmatrix} 1 & s\phi t\theta & c\phi t\theta \\ 0 & c\phi & -s\phi \\ 0 & s\phi / c\theta & c\phi / c\theta \end{bmatrix}, \quad (3)$$

where $c(\star) = \cos(\star)$, $s(\star) = \sin(\star)$ and $t(\star) = \tan(\star)$. Before we proceed, notice that $\mathbf{J}_2(\eta_2)$ yields a singularity when $\theta \to \frac{\pi}{2}$, owing to the Euler angles representation adopted in the analysis. To override such a singularity, we assume that we are operating with low pitch and roll angles, that is:

$$|\phi| \le \bar{\phi} << \frac{\pi}{2},\ |\theta| \le \bar{\theta} << \frac{\pi}{2}, \quad (4)$$

which is quite reasonable for practical cases. Furthermore, employing the standard underwater vehicle modeling properties [14], the dynamic model can be described as follows:

$$\mathbf{M}\dot{\mathbf{v}} + \mathbf{C}(\mathbf{v})\,\mathbf{v} + \mathbf{D}(\mathbf{v})\,\mathbf{v} + \mathbf{G}(\eta) = \tau + \mathbf{d}(\mathbf{t}), \quad (5)$$

where $\mathbf{M} = \mathbf{M}^T > 0$ is the diagonal inertia matrix for rigid body and added masses, $\mathbf{C}(\mathbf{v}) = -\mathbf{C}^T(\mathbf{v})$ is the coriolis and centripetal matrix, $\mathbf{D}(\mathbf{v}) > 0$ is the diagonal linear and quadratic drag matrix, $\mathbf{G}(\eta)$ involves the hydrostatic restoring forces/torques which are bounded, $\tau = [X, Y, Z, 0, 0, N]^T$ is the input (force/torque) control vector applied by the thrusters and $\mathbf{d}(t)$ is a bounded vector (i.e., $\|\mathbf{d}(t)\| \le \bar{d}, \forall t \ge 0$) representing modeling uncertainties and external disturbances (i.e., waves). Although Nessie AUV is actuated in 5 DOFs (it has no actuation in roll), in this work we only consider actuation in surge, sway, heave and yaw. Hence, Eqs. (1) and (5) formulate an underactuated dynamical system. Finally, we assume that the parameters involved in the model matrices $\mathbf{M}$, $\mathbf{C}(\mathbf{v})$, $\mathbf{D}(\mathbf{v})$ and $\mathbf{G}(\eta)$ are known (e.g., via an offline identification scheme). In what follows we formulate the problem to be solved in this work.

Robust Wall-Following Control (RWFC) Problem: *Assume that the underwater vehicle is initially placed in front of a perpendicular wall (e.g., a submerged structure). The control objective is to fix the distance x and the angle ψ from the wall as well as the depth z to some desired constant values x_d, ψ_d, z_d and maintain a desired constant velocity $\dot{y}_d$ parallel to the wall.*

It should be noted that such a task plays an important role in underwater inspection, where the vehicle has to acquire information (i.e., video, 3D modeling, fault detection, etc.) from the submerged structure.

B. State Feedback

The vehicle used in this work (Nessie VI), is equipped with various state of the art navigation sensors [15]. However, in this study only a part of these sensors were exploited and more specifically, a forward looking sonar (Tritech Gemini 720i Multi-beam Imaging Sonar), a DVL (Teledyne Explorer PA), a FOG (KVH DSP-300) and a depth sensor (Keller Series 33X). The information obtained from the DVL, the FOG or the depth sensor can be used without any further processing, while the measurement data from the sonar require further processing to extract a meaningful information (i.e. the distance and orientation of the AUV with respect to the wall).

1) Wall Detection: The forward looking sonar has a field of view of 120 degrees with a variable range extending between 0.2 and 120 meters. In the raw image data, the field of view is arranged in 256 beams, while a maximum of 25 meters range at a scale of 120 pixels per meter in the vertical bins. Even though, the Gemini 720i is known to provide a frame rate up to 30 Hz, with our setting it was only possible to achieve a 2 frames per second. Therefore, a quicker means of extracting the information is unarguably necessary to counter balance the computational burden caused by the low frame rate and the large image size.

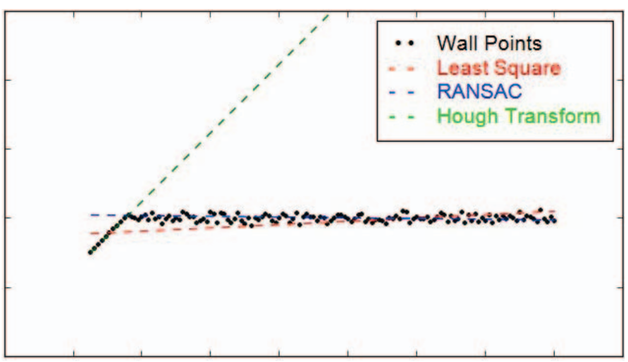

Fig. 3. Least square, Hough transform and RANSAC for synthetic data fitting.

Initially, an empirically defined threshold is applied to the raw image to identify pixels corresponding to a strong reflection. The lower range sonar readings are ignored in the subsequent processing since they are a result of the AUV body structure's reflections. The wall is assumed to be the closest object of reflection, as a result only the first non-zero bin close to the sonar is considered for the line fitting process. Finally, a RANSAC algorithm is applied on the 256 pixels of sonar beams to determine the best line representing the wall. The selection of a line fitting algorithm is done after comparing three basic line fitting techniques: least square, Hough transform and RANSAC. Fig. 3 shows the result on a synthetic acoustic image. Points in the left are perfectly represented by a straight line that diverted the Hough line towards the very few outliers, while the least square tries to compromise between these points and the rest of the data. A better result is obtained using the RANSAC algorithm,

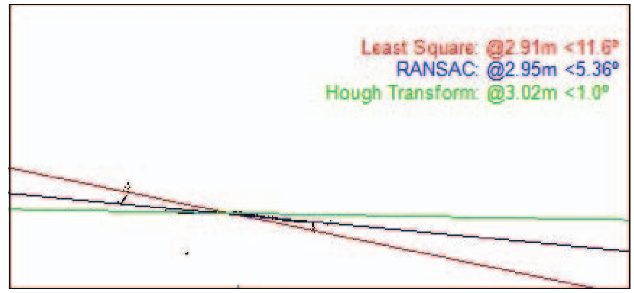

Fig. 4. Least square, Hough transform and RANSAC for sonar data fitting.

which considers part of the points in the left as outliers. A similar result is obtained in Fig. 4 for a real image acquired using the Gemini $720i$ Sonar.

2) Sensor Fusion: The sonar is a considerably very slow sensor, it delivers about twice per second (i.e., $\delta t_s \approx 0.5\,\mathrm{sec}$) in our case. As a consequence, such a low frequency raises significant issues regarding the closed loop stability and the performance of the control scheme. To alleviate this problem (i.e., to implement the control signal more frequently, that is $\delta t << \delta t_s$), we designed a sensor fusion system that utilizes both the sonar as well as the navigation measurements, that are acquired in a significantly greater frequency, to estimate the angle ψ and the distance x from the wall. More specifically, consider two consecutive time instants t_s^i, t_s^{i+1} at which the sonar delivered measurements of the angle (i.e., $\psi\left(t_s^i\right)$, $\psi\left(t_s^{i+1}\right)$) and the distance (i.e., $x\left(t_s^i\right)$, $x\left(t_s^{i+1}\right)$). Between those time instants (i.e., for all $t \in \left[t_s^i, t_s^{i+1}\right)$), we implement the control signal every δt with the updated angle and distance from the wall estimate, as follows:

$$\left.\begin{array}{l}\psi\left(t\right) = \psi\left(t_s^i\right) + \sum_{k=1}^{j} \delta\psi_k \\ x\left(t\right) = x\left(t_s^i\right) + \sum_{k=1}^{j} \delta x_k\end{array}\right\}, \forall t = t_s^i + j\delta t \in \left[t_s^i, t_s^{i+1}\right)$$

with $j = 0, 1, \ldots, \left\lfloor \frac{\delta t_s}{\delta t} \right\rfloor$ where:

$$\delta\psi_k = \frac{r\left(t_s^i + k\delta t\right) + r\left(t_s^i + (k-1)\,\delta t\right)}{2}\delta t$$

$$\delta x_k = \frac{\dot{x}\left(t_s^i + k\delta t\right) + \dot{x}\left(t_s^i + (k-1)\,\delta t\right)}{2}\delta t$$

and

$$\dot{x}\left(t\right) = \mathbf{J}_1^1\left(\eta_2\left(t\right)\right)\mathbf{v}_1\left(t\right)$$

with $\mathbf{J}_1^1\left(\eta_2\left(t\right)\right)$ denoting the first row of the Jacobian matrix (2). It can be easily verified that the proposed method updates the angle and the distance via calculating, through the trapezoidal rule (see Fig. 5), their intermediate changes $\delta\psi_k$, δx_k from the measured velocities $r\left(t\right)$, $\dot{x}\left(t\right)$ around/in the corresponding axis.

C. Control Scheme

Following common practice in the relevant literature, we initially derive a kinematic control scheme considering the actuated velocities u, v, w, r as virtual control inputs (i.e., we design some appropriate desired velocities u_d, v_d, w_d, r_d). Subsequently, the selected velocities are considered as

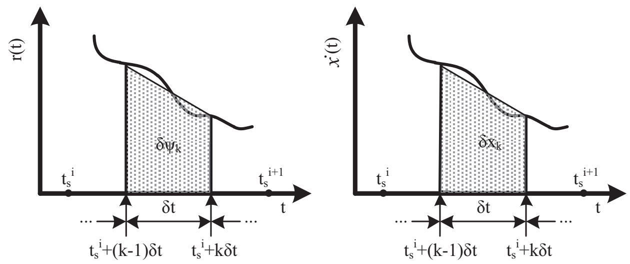

Fig. 5. The calculation of $\delta\psi_k$ and δx_k.

reference velocities in the dynamic model and the actual control inputs X, Y, Z, N are designed. However, before we proceed, notice that the evolution of the actuated degrees of freedom (i.e., surge, sway, heave, yaw) is affected by the unactuated roll and pitch motion which in turn is induced by the motion in the actuated degrees of freedom. Hence, the whole model can be viewed as two interconnected subsystems where the output of the unactuated subsystem (i.e., p, q) serves as input to the actuated one and vice versa.

In this respect, the analysis will proceed in an Input to State Stability framework, i.e., we shall first study the stability of the actuated degrees of freedom assuming that p, q are absolutely bounded by some constants $\bar{p}$, $\bar{q}$, that is:

$$|p(t)| \leq \bar{p},\ |q(t)| \leq \bar{q}, \forall t \geq 0 \tag{6}$$

and then prove that the overall closed loop system response does not violate the aforementioned bounds.

In this respect, let us first define the position and orientation errors $e_x = x - x_d$, $e_z = z - z_d$ and $e_\psi = \psi - \psi_d$. Notice, however, that we have not defined a position error in y-axis since: i) we require constant velocity $\dot{y}_d$ in this axis and ii) an accurate estimate of y is almost impossible in the absence of absolute position measurements. To proceed, we select the following kinematic controller:

$$\begin{gathered}\begin{bmatrix} u_d \\ v_d \\ w_d \end{bmatrix} = \mathbf{J}_1^{-1}(\eta_2) \begin{bmatrix} -k_x e_x \\ \dot{y}_d \\ -k_z e_z \end{bmatrix} \\ r_d = -2k_\psi \tfrac{c\theta}{c\phi} e_\psi \end{gathered} \tag{7}$$

with k_x, k_z, $k_\psi > 0$ and we design the control inputs as follows:

$$\begin{aligned}\begin{bmatrix} X \\ Y \\ Z \\ N \end{bmatrix} = \bar{\mathbf{M}} \begin{bmatrix} \dot{u}_d \\ \dot{v}_d \\ \dot{w}_d \\ 0 \\ 0 \\ \dot{r}_d \end{bmatrix} + \left(\bar{\mathbf{C}}(\mathbf{v}) + \bar{\mathbf{D}}(\mathbf{v})\right) \begin{bmatrix} u_d \\ v_d \\ w_d \\ 0 \\ 0 \\ r_d \end{bmatrix} + \bar{\mathbf{G}}(\eta) \\ - \begin{bmatrix} k_u e_u \\ k_v e_v \\ k_w e_w \\ k_r e_r \end{bmatrix} - \begin{bmatrix} \mathbf{J}_1^T(\eta_2) \begin{bmatrix} e_x \\ 0 \\ e_z \end{bmatrix} \\ \tfrac{c\phi}{c\theta} e_\psi \end{bmatrix}\end{aligned} \tag{8}$$

where $\bar{\mathbf{M}}$, $\bar{\mathbf{C}}(\mathbf{v})$, $\bar{\mathbf{D}}(\mathbf{v})$ and $\bar{\mathbf{G}}(\eta)$ involve the rows of the corresponding model matrices in (5), concerning only the actuated degrees of freedom (i.e., u, v, w, r). Finally, k_u, k_v, k_w, k_r are positive control gains and $e_u = u - u_d$, $e_v = v - v_d$, $e_w = w - w_d$, $e_r = r - r_d$ denote the velocity errors.

The following theorem summarizes the main results of this work.

Theorem 1: Consider an underwater vehicle described by (1), (5) and the control scheme (7), (8). There exist positive control gains k_x, k_z, k_ψ, k_u, k_v, k_w, k_r such that the proposed control scheme solves the RWFC Problem presented in Subsection II-A despite the presence of modeling uncertainties and external disturbances.

Proof: Consider the following Lyapunov function candidate for the position/orientation errors:

$$L_1 = \frac{1}{2}\left(e_x^2 + e_z^2 + e_\psi^2\right).$$

Differentiating with respect to time, substituting (1) and utilizing the fact that $u = e_u + u_d$, $v = e_v + v_d$, $w = e_w + w_d$, $r = e_r + r_d$ with u_d, v_d, w_d, r_d as defined in (7), we arrive at:

$$\begin{aligned}\dot{L}_1 = -k_x e_x^2 - k_z e_z^2 - 2k_\psi e_\psi^2 + [e_x, 0, e_z]\,\mathbf{J}_1(\eta_2) \begin{bmatrix} e_u \\ e_v \\ e_w \end{bmatrix} \\ + e_\psi \frac{c\phi}{c\theta} e_r + e_\psi \frac{s\phi}{c\theta} q\,.\end{aligned}$$

Employing (4), (6) and completing the squares, we obtain:

$$\begin{aligned}\dot{L}_1 \leq -k_x e_x^2 - k_z e_z^2 - k_\psi e_\psi^2 + [e_x, 0, e_z]\,\mathbf{J}_1(\eta_2) \begin{bmatrix} e_u \\ e_v \\ e_w \end{bmatrix} \\ + e_\psi \frac{c\phi}{c\theta} e_r + \frac{\bar{q}^2}{4k_\psi \cos\left(\bar{\theta}\right)}\,.\end{aligned} \tag{9}$$

Let us now augment L_1 with a corresponding velocity error term:

$$L_2 = \frac{1}{2}\mathbf{e}_\mathbf{v}^T \mathbf{M} \mathbf{e}_\mathbf{v},$$

where $\mathbf{M}$ is the positive definite inertia matrix and $\mathbf{e}_\mathbf{v} = [e_u, e_v, e_w, p, q, e_r]^T$ is the velocity error vector (since the stabilization of the unactuated degrees of freedom p, q is required, notice that the velocity error $\mathbf{e}_\mathbf{v}$ involves directly those states). Subsequently, we define the overall Lyapunov function candidate $L = L_1 + L_2$. Differentiating L with respect to time and substituting (5), (9) and the control scheme (8), we get:

$$\begin{aligned}\dot{L} \leq & -k_x e_x^2 - k_z e_z^2 - k_\psi e_\psi^2 - \mathbf{e}_\mathbf{v}^T \mathbf{C}(\mathbf{v})\,\mathbf{e}_\mathbf{v} \\ & - \mathbf{e}_\mathbf{v}^T\left(\mathbf{D}(\mathbf{v}) + \mathbf{K}_\mathbf{v}\right)\mathbf{e}_\mathbf{v} - e_v^T\left(\underline{\mathbf{G}}(\eta_2) + \mathbf{d}(t)\right) \\ & + \frac{\bar{q}^2}{4k_\psi \cos\left(\bar{\theta}\right)}\end{aligned}$$

where $\mathbf{K}_\mathbf{v} = \text{diag}([k_u, k_v, k_w, 0, 0, k_r])$ and $\underline{\mathbf{G}}(\eta_2) = [0, 0, 0, G_4(\eta_2), G_5(\eta_2), 0]^T$ with $G_4(\eta_2)$, $G_5(\eta_2)$ denoting the 4$^{\text{th}}$ and 5$^{\text{th}}$ element of the matrix $\mathbf{G}(\eta_2)$. Employing: i) the skew symmetry of $\mathbf{C}(\mathbf{v})$, ii) the diagonallity and positive definiteness of $\mathbf{D}(\mathbf{v})$ as well as iii) the boundedness

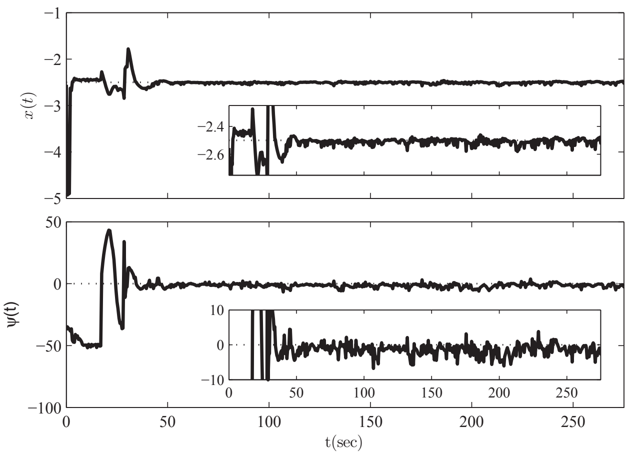

Fig. 6. No disturbances: The distance (m) and orientation (deg) with respect to the wall along with the desired values.

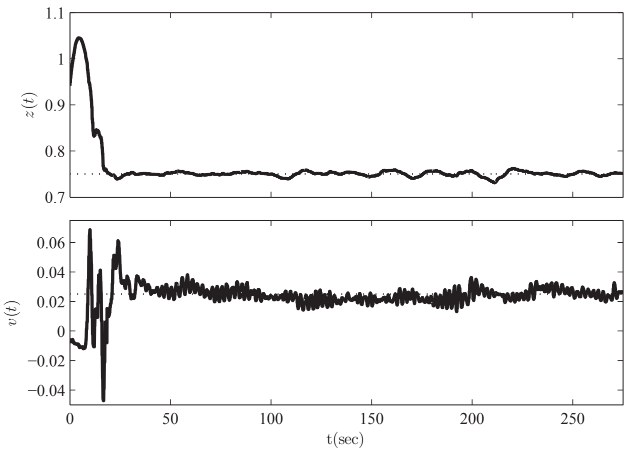

Fig. 7. No disturbances: The depth (m) and the velocity (m/s) in the y axis (parallel to the wall) along with the desired values.

of $\underline{\mathbf{G}}(\eta_2)$ and $\mathbf{d}(t)$ (i.e., $\|\underline{\mathbf{G}}(\eta_2)\| \leq \bar{G}$ and $\|\mathbf{d}(t)\| \leq \bar{d}$, $\forall t \geq 0$), and completing the squares, we finally arrive at:

$$\dot{L} \leq -k_x e_x^2 - k_z e_z^2 - k_\psi e_\psi^2 - k_v \|\mathbf{e_v}\|^2 + \frac{(\bar{G}+\bar{d})^2}{4k_v} + \frac{\bar{q}^2}{4k_\psi \cos(\bar{\theta})}$$

where $k_v = \frac{1}{2}\lambda_{\min}(\mathbf{D}(\mathbf{v}) + \mathbf{K_v})$. Therefore, we conclude that $\dot{L} \leq 0$ when either $|e_x| > \sqrt{d/k_x}$ or $|e_z| > \sqrt{d/k_z}$ or $|e_\psi| > \sqrt{d/k_\psi}$ or $\|\mathbf{e_v}\| > \sqrt{d/k_v}$, with $d \equiv \frac{(\bar{G}+\bar{d})^2}{4k_v} + \frac{\bar{q}^2}{4k_\psi \cos(\bar{\theta})}$. Thus, e_x, e_z, e_ψ, $\mathbf{e_v}$ are uniformly ultimately bounded with respect to the sets $E_x = \left\{e_x \in \Re : |e_x| \leq \sqrt{d/k_x}\right\}$, $E_z = \left\{e_z \in \Re : |e_z| \leq \sqrt{d/k_z}\right\}$, $E_\psi = \left\{e_\psi \in \Re : |e_\psi| \leq \sqrt{d/k_\psi}\right\}$ and $E_v = \left\{\mathbf{e_v} \in \Re^6 : \|\mathbf{e_v}\| \leq \sqrt{d/k_v}\right\}$ respectively. As a result, by adjusting appropriately the control gains k_x, k_z, k_ψ, k_u, k_v, k_w, k_r we may achieve convergence of the errors to a sufficiently small neighborhood of the origin and consequently solve the RWFC Problem.

However, the above results hold under the assumption that $|p(t)| \leq \bar{p}$, $|q(t)| \leq \bar{q}$, $\forall t \geq 0$. Therefore, we need to establish that the proposed control scheme does not violate the aforementioned bounds. In this direction, let us define the set:

$$E = \left\{(e_x, e_z, e_\psi, \mathbf{e_v}) \in \Re^9 : L \leq \bar{L}\right\}$$

where $\bar{L}$ is chosen as the largest constant for which $|p| \leq \bar{p}$, $|q| \leq \bar{q}$, $\forall (e_x, e_z, e_\psi, \mathbf{e_v}) \in E$. Subsequently, for sufficiently large control gains k_x, k_z, k_ψ, k_u, k_v, k_w, k_r it can be easily verified that $E_x \times E_z \times E_\psi \times E_v \subset E$ (as it was mentioned earlier, the size of the sets E_x, E_z, E_ψ, E_v can be reduced by increasing the control gains in the direction of achieving satisfactory tracking performance). Hence, for all $(e_x(0), e_z(0), e_\psi(0), \mathbf{e_v}(0)) \in E$, it follows that L is bounded from above by $\bar{L}$, $\forall t \geq 0$ since $\dot{L} \leq 0$, $\forall (e_x, e_z, e_\psi, \mathbf{e_v}) \in E - (E_x \times E_z \times E_\psi \times E_v)$, which implies that $(e_x(t), e_z(t), e_\psi(t), \mathbf{e_v}(t)) \in E$, $\forall t \geq 0$, where $|p| \leq \bar{p}$, $|q| \leq \bar{q}$ hold true, thus completing the proof.

III. EXPERIMENTS

In order to prove the overall efficiency of the proposed system, two experimental procedures where carried out. The experiments took place inside a water tank using the Nessie VI AUV. Initially, a rough dynamic model of Nessie VI was obtained via an off-line identification procedure. The first experiment was conducted without external disturbances whereas the second in the presence of medium height waves, which were produced by the test tank oscillating mechanism. In both cases the vehicle starts from an arbitrary initial configuration with at least a part of the wall visible by the Multi-beam Imaging Sonar. The goal is to follow the wall by keeping a fixed distance of $x_d = 2.5m$ and $\psi_d = 0^o$ orientation with respect to the wall, while moving alongside the wall with a constant velocity $\dot{y}_d = 0.025m/s$ at a constant depth $z_d = 0.75m$. The vehicle's response can be affected by the waves only when operating close to surface. Thus, the desired depth is set relatively low. Finally, the control gains were selected as follows: $k_x = 0.7$, $k_z = 0.5$, $k_\psi = 0.35$, $k_u = 0.5$, $k_v = 0.2$, $k_w = 0.5$, $k_r = 0.5$.

A. No external disturbances

In this experiment, the vehicle performs the sonar servoing scheme without external disturbances. The response of the distance x and the orientation ψ with respect to the wall are shown in Fig.6. The response along z axis is depicted in Fig. 7. As it was predicted by the theoretical analysis and proven by the experimental procedure, the states of the vehicle asymptotically converge to the desired values. The maximum error at the steady state is no more than $\pm 5cm$ along x axis, $\pm 5^o$ about z axis and $\pm 3cm$ along z axis. It can also be observed in Fig.7, that due to the velocity controller along y axis, the parallel to the wall velocity converges to the desired value with maximum error $\pm 0.005m/s$. Thus, a smooth surveillance trajectory is achieved.

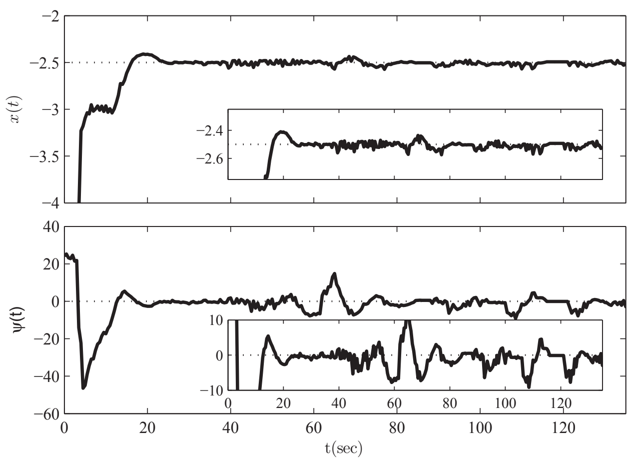

Fig. 8. In the presence of disturbances (medium height waves): The distance (m) and orientation (deg) with respect to the wall along with the desired values.

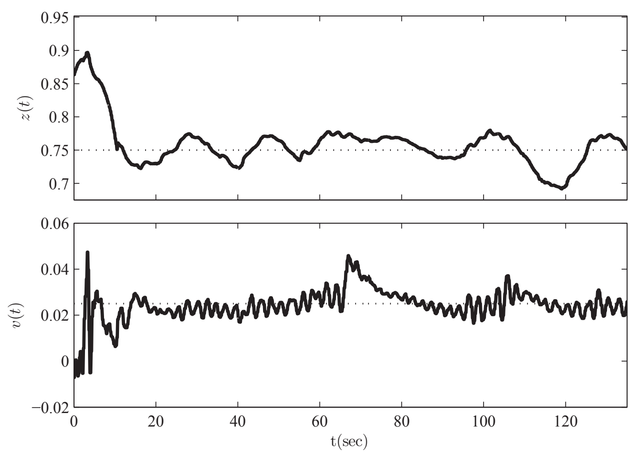

Fig. 9. In the presence of disturbances (medium height waves): The depth (m) and the velocity (m/s) in the y axis (parallel to the wall) along with the desired values.

B. External disturbances

In this experiment, the same scenario as in Subsection III-A is conducted, but with the wave creation mechanism of the test tank enabled. It should be noted here, that the control scheme does not have any prior knowledge of the external disturbances (amplitude and frequency). The response of the position along x axis and the orientation ψ with respect to the wall are shown in Fig.8. The response along z axis and the velocity in y axis are depicted in Fig. 7. As it proven by the experimental procedure, the controller deals with the external disturbances in a satisfactory manner. The vehicle states asymptotically converge to the desired values but with more oscillations relatively to the disturbance free scenario. The maximum error in steady state is no more than $\pm 8cm$ along x axis, $\pm 10^o$ about z axis and $\pm 5cm$ along z axis. As it can be seen in Fig.9, sway velocity error can reach $\pm 0.02m/s$ although in most cases the velocity error is kept below $\pm 0.005m/s$. In any case, a suitable surveillance trajectory is achieved, even in the case of external disturbances.

IV. Conclusions

This paper describes the design and implementation of a sonar-servoing control scheme for an Autonomous Underwater Vehicle. The sensor suite includes a Multi-beam Imaging Sonar which provides measurements to a RANSAC-based algorithm for structure detection and pose estimation of the vehicle with respect to the structure. Subsequently, the sonar-based pose estimation is properly fused with the measurements provided by the rest of the navigation sensors (DVL and FOG). The proposed control scheme has analytically guaranteed stability and convergence properties, while it is robust against external disturbances and parametric uncertainties in the AUV dynamic model. The efficiency of the overall system, is demonstrated using the Nessie VI AUV in the presence of external disturbances (medium height waves).

References

[1] K. D. Do and J. Pan, *Control of Ships and Underwater Vehicles: Design for Underactuated and Nonlinear Marine Systems*. Springer-Verlag, London, 2009.

[2] S. Wadoo and P. Kachroo, *Autonomous Underwater Vehicles: Modeling, Control Design and Simulation*. Taylor and Francis Group, Boca Raton, 2011.

[3] T. I. Fossen, *Handbook of Marine Craft Hydrodynamics and Motion Control*. John Wiley and Sons, Chichester, 2011.

[4] H. Johannsson, M. Kaess, B. Englot, F. Hover, and J. Leonard, "Imaging sonar-aided navigation for autonomous underwater harbor surveillance," in *IEEE/RSJ 2010 International Conference on Intelligent Robots and Systems, IROS 2010*, 2010, pp. 4396–4403.

[5] D. Nad, N. Miskovic, V. Djapic, and Z. Vukic, "Sonar aided navigation and control of small uuvs," in *2011 19th Mediterranean Conference on Control and Automation, MED 2011*, 2011, pp. 418–423.

[6] Y. Yang and D. Zhu, "Research on dynamic path planning of auv based on forward looking sonar and fuzzy control," in *Proceedings of the 2011 Chinese Control and Decision Conference, CCDC 2011*, 2011, pp. 2425–2430.

[7] M. Pinto, B. Ferreira, A. Matos, and N. Cruz, "Using side scan sonar to relative navigation," in *MTS/IEEE Biloxi - Marine Technology for Our Future: Global and Local Challenges, OCEANS 2009*, 2009.

[8] E. Thurman, J. Riordan, and D. Toal, "Integrated control of multiple acoustic sensors for optimal seabed surveying," in *IFAC Proceedings Volumes (IFAC-PapersOnline)*, vol. 7, 2007, pp. 367–372.

[9] P. . Lee, B. . Jun, J. . Li, H. T. Choi, K. Kim, S. . Kim, C. . Lee, S. . Han, B. . Gu, S. . Lee, H. . Chung, and H. S. Choi, "Navigation and control system of a deep-sea unmanned underwater vehicle 'hemire'," in *OCEANS 2006 - Asia Pacific*, 2007.

[10] W. Kazmi, P. Ridao, D. Ribas, and E. Hernández, "Dam wall detection and tracking using a mechanically scanned imaging sonar," in *IEEE International Conference on Robotics and Automation*, 2009, pp. 3228–3233.

[11] I. Ruiz, Y. Petillot, D. Lane, and C. Salson, "Feature extraction and data association for auv concurrent mapping and localisation," in *IEEE International Conference on Robotics and Automation*, 2001, pp. 2785–2790.

[12] E. Trucco, Y. Petillot, I. Ruiz, K. Plakas, and D. Lane, "Feature tracking in video and sonar subsea sequences with applications," *Computer Vision and Imaging Understanding*, pp. 92–122, 2000.

[13] V. Nguyen, S. Gächter, A. Martinelli, N. Tomatis, and R. Siegwart, "A comparison of line extraction algorithms using 2d range data for indoor mobile robotics," *Auton. Robots*, pp. 97–111, 2007.

[14] T. I. Fossen, *Guidance and Control of Ocean Vehicles*. Wiley, New York, 1994.

[15] R. Baxter, J. Cartwright, J. Clay, O. Clert, B. Davis, J. Lopez, F. Maurelli, Y. Petillot, P. Patrón, and N. Valeyrie, "Nessie v autonomous underwater vehicle," *Student Autonomous Underwater Competition - Europe (SAUC-E)*, 2010.